A practical technique for the generation of highly uniform LIPSS

Ardron, Marcus; Weston, Nick; Hand, Duncan Paul

Published in:
Applied Surface Science

DOI:
10.1016/j.apsusc.2014.05.154

Publication date:
2014

Applied Surface Science xxx (2014) xxx–xxx

Contents lists available at ScienceDirect

Applied Surface Science

journal homepage: www.elsevier.com/locate/apsusc

A practical technique for the generation of highly uniform LIPSS

Marcus Ardron [a,b,*], Nick Weston [b], Duncan Hand [a]

[a] School of Engineering & Physical Sciences, Heriot Watt University, Edinburgh EH14 4AS, UK
[b] Renishaw PLC, Research Avenue North, Riccarton, Edinburgh EH14 4AP, UK

ARTICLE INFO

Article history:
Received 4 November 2013
Received in revised form 22 April 2014
Accepted 23 May 2014
Available online xxx

Keywords:
LIPSS
Nanoripples
Roughness
Stainless steel
Polishing

ABSTRACT

Laser-induced periodic surface structures (LIPSS) can be reliably produced with ultrashort (<10 ps) laser pulses given fluence near the ablation threshold. Neat, parallel, uniform structures are harder to reproduce. Electrodynamic models show a field at normal incidence interacts with the surface resulting in periodicity in intensity along the surface in the direction of the incident E-field producing ridges and toughs on the surface orthogonal to the E-field. A completely smooth surface offers nothing to perturb the eventual periodic feature formation but is very difficult to achieve: we have demonstrated that simply avoiding surface roughness components near the frequency and direction of the emergent features significantly improves uniform feature production. An appropriate unidirectional polishing process can be realised using an inexpensive spinning cloth wheel. By using a cylindrical lens we were also able to process stainless steel surfaces at 5 $mm^2\ s^{-1}$ so indicating useful industrial potential.

1. Introduction

The periodic features that emerge on material surfaces after a number of laser pulses near the ablation threshold are commonly known as laser-induced periodic surface structures (LIPSS) [1,2] and have been produced with a wide range of pulse lengths on a broad selection of materials. These structures have interesting and potentially useful properties: nano-structures can be used to affect the functional properties of surfaces such as wetting [3], optical properties [4], or friction control [5]; however, a reliable and quick method of fabrication is essential if they are to be exploited in real applications. Although the laser writing process is quite straightforward, unless the initial surface is very finely polished the generated periodic features are not completely uniform but instead are modified by initial random scratches on the surface [6], for example see Fig. 1. In this paper we describe and explain (with reference to theory) a simple technique to ensure highly uniform LIPSS features which avoids the time-consuming step of fine surface polishing. It has been shown that LIPSS can be helpful in control of friction and wetting [3,7,8] but many engineering applications, such as injection moulds and some bearing surfaces, can have geometry that does not lend itself to very fine surface finishing prior to laser treatment. In principle a much lower quality surface will still allow uniform LIPSS to occur if linear polishing marks are aligned with the laser E-field so opening a wide range of applications to this technology.

At least two types of LIPSS can occur from ultrashort pulse interaction; high spatial frequency LIPSS (HSFL) [9,10] and low spatial frequency LIPSS (LSFL). This paper deals with only LSFL despite using ultrashort pulses (well below the pulse duration at which the fluence required for material breakdown scales with $\sqrt{\tau_{pulse}}$ [11], specifically $\tau_{pulse} < 10$ ps).

2. Theory

Many theories have been developed since the first publication about this phenomenon in 1965 [12] with surface plasmons [13] and mechanical wave motion [14] offering potentially robust mechanisms. Detailed electrodynamic models are represented by the efficacy factor theory (EFT) [15] and the finite difference time domain (FDTD) method [16]; the latter being a numerical interpretation of the first is unfortunately somewhat opaque and so does not provide the same physical insight into the formation process as an analytical method. We therefore used EFT to guide development of the production process. EFT examines the interaction of an electromagnetic plane wave with a rough surface, and calculates the resultant energy absorption just below the surface.

For geometric simplicity we consider light at normal incidence to a plane surface which was at the focal distance from the final lens so the electromagnetic field at the surface is planar. A cross-section is taken as shown in Fig. 2 and this is split into 3 regions: (i) the dielectric space above, (ii) selvedge: a thin region containing

* Corresponding author at: School of Engineering & Physical Sciences, Heriot Watt University, Edinburgh EH14 4AS, UK. Tel.: +44 0131 451 4146.
E-mail addresses: ma745@hw.ac.uk, marcus.ardron@renishaw.com (M. Ardron).

http://dx.doi.org/10.1016/j.apsusc.2014.05.154

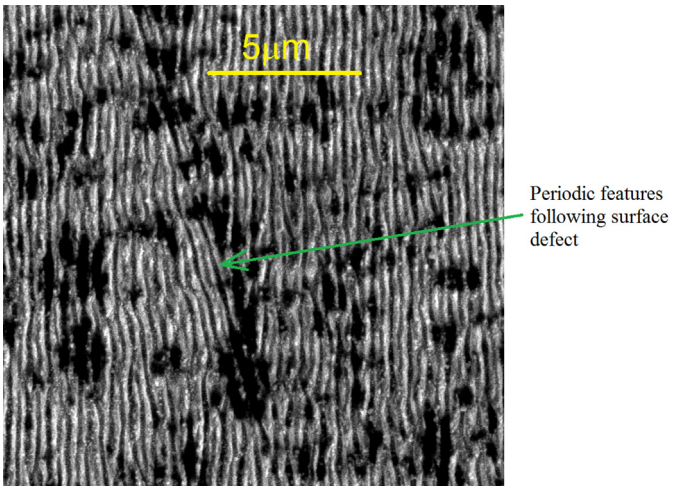

Fig. 1. LIPSS features on stainless steel (Sandvik Chromflex) demonstrating the impact of pre-existing surface imperfections. A diagonal scratch causes some of the features to follow the disruption rather than the adjacent features.

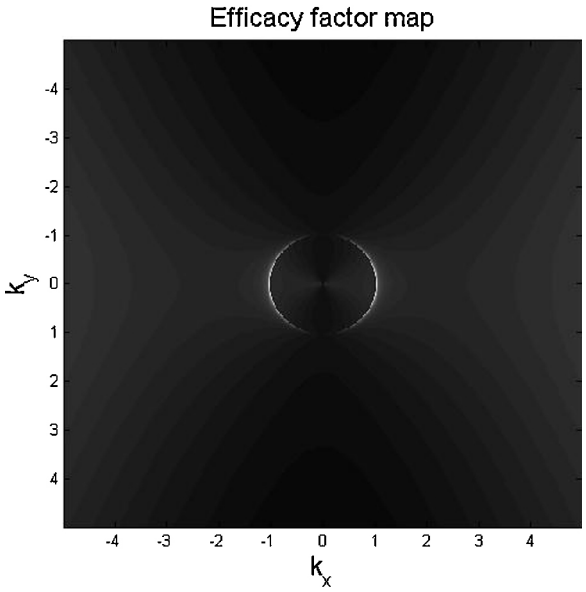

Fig. 3. Efficacy factor map for 800 nm light normally incident on stainless steel with effective index of refraction $\tilde{n} = 2.0 + 5.9i$. The spatial frequencies are normalised to the laser optical frequency. Light crescent shapes represent efficacy factor peaks at close to the laser wavelength and predominantly aligned with the *x*-axis.

the (rough) surface, and (iii) the solid material below the surface. Expressions have been developed by Sipe et al. [15] in the derivation of EFT to describe the field in each of these regions to give the energy absorption just below the surface; spatial frequency peaks in this field were correlated with experimental observations of LIPSS [17]. The key equation is:

$$\mathbf{A}(\vec{\kappa}) \propto \eta(\vec{\kappa};\ \vec{\kappa})|b(\vec{\kappa})|$$

where $A(\vec{\kappa})$ represents the absorbed energy just below the surface; $\eta(\vec{\kappa};\vec{\kappa})$ is the efficacy factor due to the incident beam (characterised by $\vec{\kappa}_l$, the component of the incident wave vector parallel to the surface) interacting with the surface; $b(\vec{\kappa})$ is the Fourier representation of the surface roughness; and $\vec{\kappa}$ represents spatial frequency parallel to the surface in the *x*–*y* plane. Spatial frequencies are normalised by the frequency of incident light. Surface modification is presumed to be dependent on the existence of amplitude peaks in $A(\vec{\kappa})$ which require non-zero regions of $\eta(\vec{\kappa};\vec{\kappa}_l)$ and $b(\vec{\kappa})$ to overlap at one or more **s**patial frequencies: suitable spatial frequency components must exist in the surface topography before LIPSS can evolve. Deviations from a smooth plane scatter incident light and here introduce oscillatory field components along the surface; indeed, single defects lead to local nanostructures with low pulse numbers which can merge with those from neighbouring defects after many more pulses [18]. In essence, surface plasmons need something to 'kick off' from. A completely smooth surface suffers random damage due the first pulse or two from an intense laser [19]. Further pulses are then scattered [20] and frequency components of roughness can now couple with scattered light components along the surface to give distinct peaks in the absorbed energy [21].

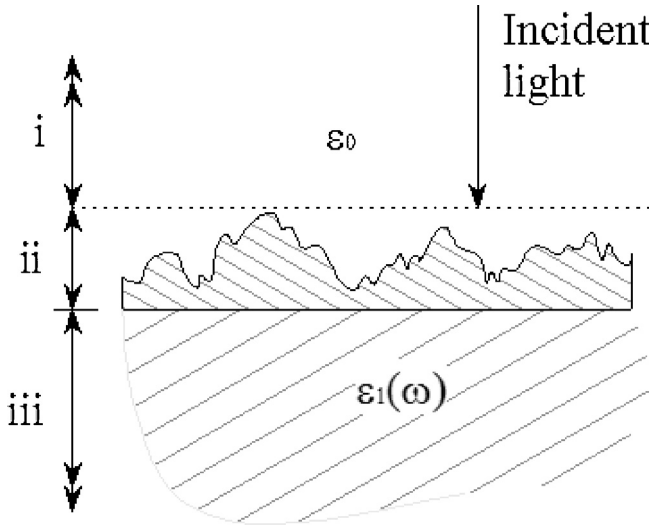

Fig. 2. Surface cross section split into three regions: (i) dielectric, (ii) selvedge, and (iii) bulk material.

Any imperfections in the surface, such as scratches, modify the absorption and result in distortion of the emergent LIPSS [15]. According to the EFT equation above, any spatial frequency components orthogonal to those in the efficacy factor will not affect the resultant absorption; from this we deduce that high quality, uniform LIPSS are best formed on a surface polished *orthogonally* to the direction of intended LIPSS periodicity. In general, polishing is carried out using a circular motion which results in polishing marks in all directions across the surface which can only be removed by polishing to a really fine scale. Linear polishing, however, can remove pre-existing features in other directions, leaving only polishing marks in a single direction. Although contradictions are found in the literature, it is our experience that the direction of emergent low spatial frequency (LSFL) periodicity is parallel to the E-field of the incident laser energy (i.e. the direction of the ridges themselves is orthogonal to the E-field).

Peaks in the efficacy factor map do occur for smooth surfaces but require a roughness component at the same frequency to lead to absorption. Taking the conductivity of stainless steel at room temperature as $\sigma_{ss} = 1.4 \times 10^6\ \Omega^{-1}\ m^{-1}$ [22] and free electron density of $8.5 \times 10^{28}\ m^{-3}$ (based on density of $7874\ kg\ m^{-3}$ and assuming molar mass as that of iron) the Drude model [13] leads to a time constant (or momentum scattering time[23]) of 0.56×10^{-15} s which was used to obtain an effective refractive index of $\tilde{n} = 2.0 + 5.9i$. Employing a numerical evaluation of EFT coded from [15,24] with normally incident light of $\lambda = 800$ nm wavelength onto a smooth surface (roughness fill-factor $F = 0$), the efficacy factor map has crescent shaped peaks with a radius of about $|k| = 1$ and centroids on $k_y = 0$ (see Fig. 3). Preferential absorption can occur if peaks in the

Please cite this article in press as: M. Ardron, et al., A practical technique for the generation of highly uniform LIPSS, Appl. Surf. Sci. (2014), http://dx.doi.org/10.1016/j.apsusc.2014.05.154

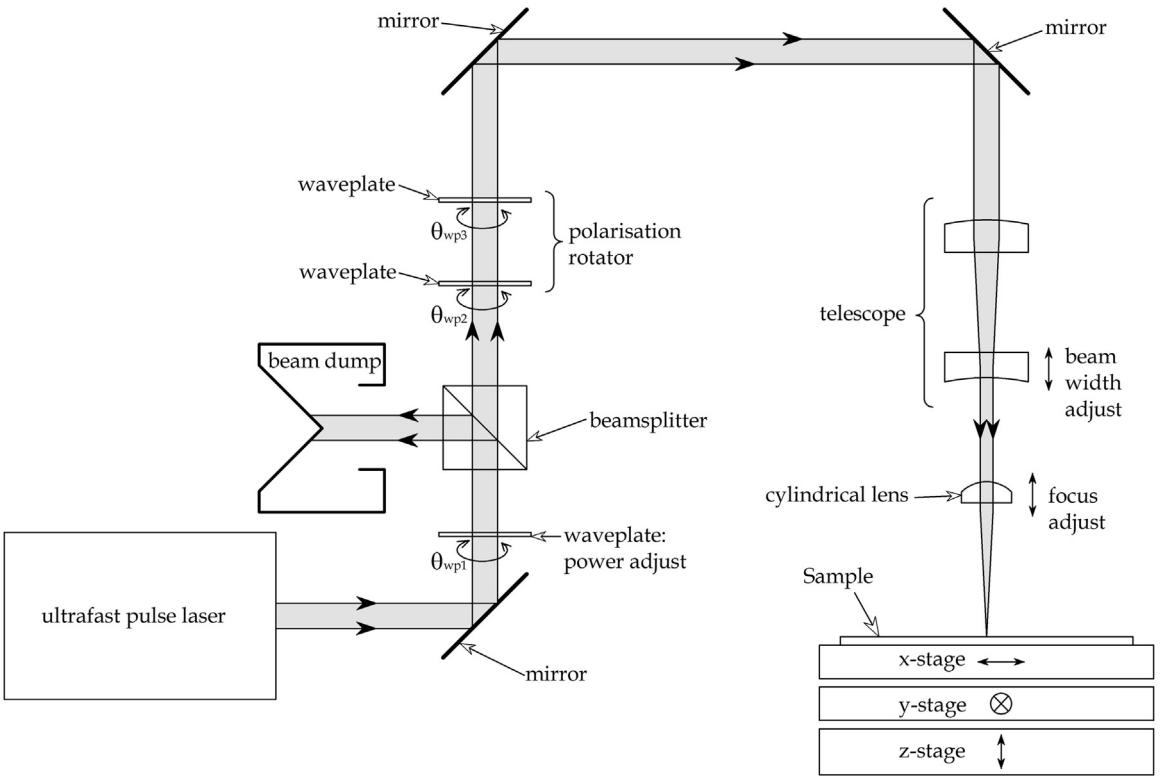

Fig. 4. Apparatus layout. Waveplate 1 is used for power adjustment and the distance between telescope lenses for beam width adjustment. Waveplates 2 and 3 were used to set polarisation orientation and form (linear, circular or elliptical).

roughness map coincide with any points on these crescents and over a number of pulses surface texture tends to be pulled towards the centroid of each crescent; the role of feedback was suggested in [25]. With no initial surface roughness one may expect random surface modification because after the pulse there are variations in the energy of free electrons depending on depth below the surface, direction of travel during pulse interaction and screening caused by surrounding electrons (using the electron gas model for this metal). Multi-photon absorption further complicates this matter and also alters the simple Drude model by energy transfer of multiple photon energies. This is not considered here.

3. Experiment

Whereas low spatial frequency LIPSS ($\Lambda \sim 0.8\lambda$) have been produced with pulse lengths spanning the entire commercially available range of lasers [12,17,26], we chose to use ultrashort pulses in common with the vast majority of published successful studies. The laser used was a Spectra Physics Hurricane which provides an average power of about 800 mW at 800 nm for a pulse length of ~120 fs at 5 kHz. The Gaussian (TEM_{00}) beam from the laser was measured to have a diameter of 11.7 mm to $1/e^2$ and was then focused through a 50 mm cylindrical lens to give a line focus and passes through a 2 mm wide aperture to cause ablation over an area of approximately 2 mm by 5 μm.

Mannion et al. showed that, with similar laser parameters, low pulse numbers caused ablation and LIPSS on stainless steel 316 at a fluence of 0.42 J cm^{-2} [27] suggesting that about one quarter of our pulse energy was at sufficient intensity to cause ablation. Other work by the same group found the ablation fluence of stainless steel for 100 pulses to be 0.16 J cm^{-2} [28]; also Orzi et al. measured it to be 0.15 ± 0.03 J cm^{-2} [29] but it must be noted that single pulse ablation threshold is higher than that for many pulses [27] and for a Gaussian intensity profile only part of the beam will be above the ablation threshold. In practise a waveplate and beam splitter were used during experimental trails to set the fluence so that slight ablation was just measureable after a single pulse.

The experimental arrangement is shown in Fig. 4. The workpiece was moved at a constant velocity below the final lens in the direction of the narrow dimension of the focus; hence the number of

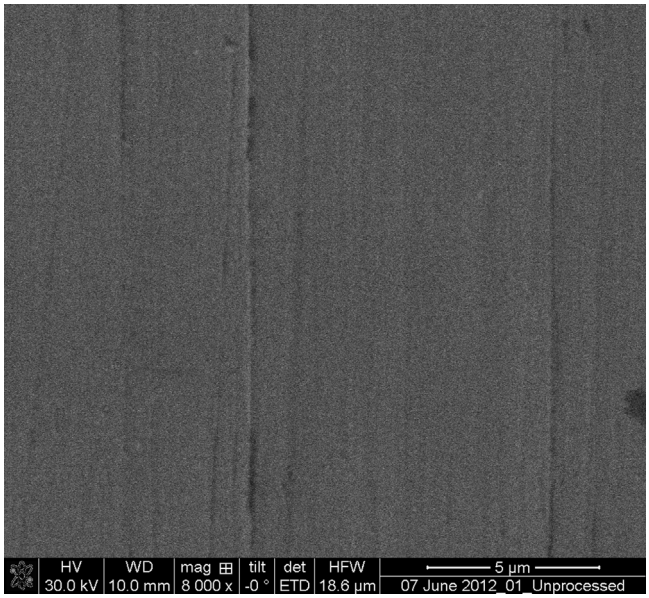

Fig. 5. SEM image of surface prepared by brief linear polishing process. The surface is quite smooth in the vertical direction.

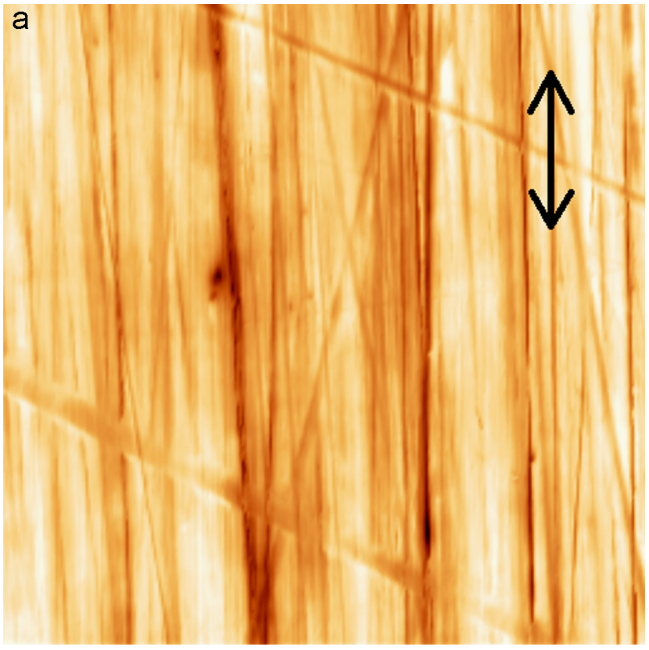

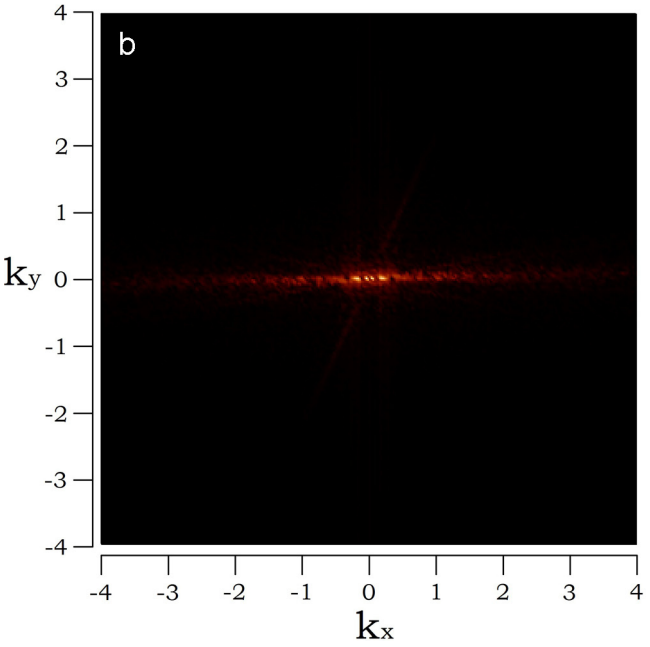

Fig. 6. (a) Left, AFM scan of 20 μm square area showing primarily vertical polishing marks (arrow indicates direction of polishing); (b) right, shows the corresponding modulus of the Fourier Transform (with frequency axes normalised to the laser wavenumber) indicating negligible frequency content in the vertical direction in contrast to significant content in the horizontal direction, mostly at lower wavenumber than the incident beam, i.e. $|k| < 1$.

pulses incident on any area of the surface is controlled by the surface velocity according to: $N = f \cdot w/v$, where w is the beam width at the surface (taken as the width of visible damage to the workpiece from a single pulse), f is the laser repetition rate and v the scan speed. A region 2 mm wide could hence be treated in a single pass. The polarisation was set to align the E-field parallel to the narrow dimension of the focus with the aim of making ~2 mm wide ripples with repeating structures occurring over the entire length of any given production scan. Taking the cylindrical lens focal length of 50 mm the calculated peak fluence was 0.37 J cm^{-2} based on pulse energy of 150 μJ, beam diameter of 11.7 mm to $1/e^2$ and assuming

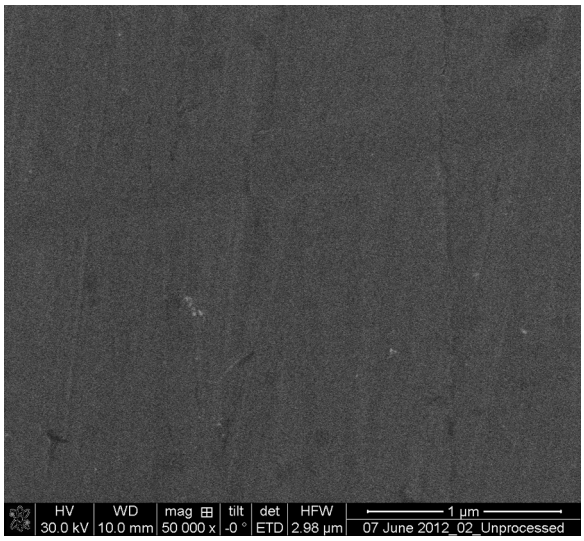

Fig. 7. Polished surface at 50,000× shows no sign of roughness. The apparently smooth surface would show roughness if viewed on a larger scale, only appearing smooth at this high magnification chosen to span a range around the laser wavenumber.

Gaussian intensity profile. The material used was a high fatigue strength stainless steel, Sandvik Chromflex 7C27Mo2, representative of a durable engineering material suitable for replication tooling or direct application. The thickness used was 1 mm, cut into strips 15 mm by 100 mm. The focal position was aligned aurally (maximum audible disruption from laser incident on workpiece), at which point plasma formation was also visible at the sample surface. A long running industrial process using similar equipment has shown focus repeatability gives feature widths of 7 ± 1 μm using the aural focus finding technique for many hundreds of runs.

To decouple polishing marks from LIPSS formation, the strip material was linearly polished (as discussed above) using a spinning cloth wheel and 'soap' type polishing compound. Given that the writing laser has a wavelength of around 800 nm one can expect periodic structures with a periodicity of just below 800 nm, so the surface would ideally be smooth at this length-scale. The linearly polished material was analysed using both an SEM and an AFM (examples shown in Figs. 5 and 6(a), respectively, the polishing direction in these images being vertical). Visually, these surfaces are far from high quality specular faces; however, compared to the expected LIPSS, the remaining surface features are shallow, low frequency and orthogonally aligned. The roughness was measured to have an average of $Ra \approx 10$ nm and RMS of $Rq \approx 11.8$ nm, both over the 50 μm measuring window; somewhat smaller than the intended depth of the LIPSS at >50 nm. A surface examined using the AFM is presented Fig. 6(a) together with Fourier analysis in Fig. 6(b), which shows no significant amplitude in the y direction and hence no overlap with potential peaks in $\eta(\bar{\kappa}; \bar{\kappa}_l)$. Also, in the x direction the main peaks are at a lower spatial frequency than that associated with the laser wavelength.

4. Results

A series of areas were treated with different velocities of affect a range of pulse numbers incident in the treated surface. The Gaussian intensity profile of the scanned laser means the number of pulses is not an exact figure, more of a scaling parameter.

Please cite this article in press as: M. Ardron, et al., A practical technique for the generation of highly uniform LIPSS, Appl. Surf. Sci. (2014), http://dx.doi.org/10.1016/j.apsusc.2014.05.154

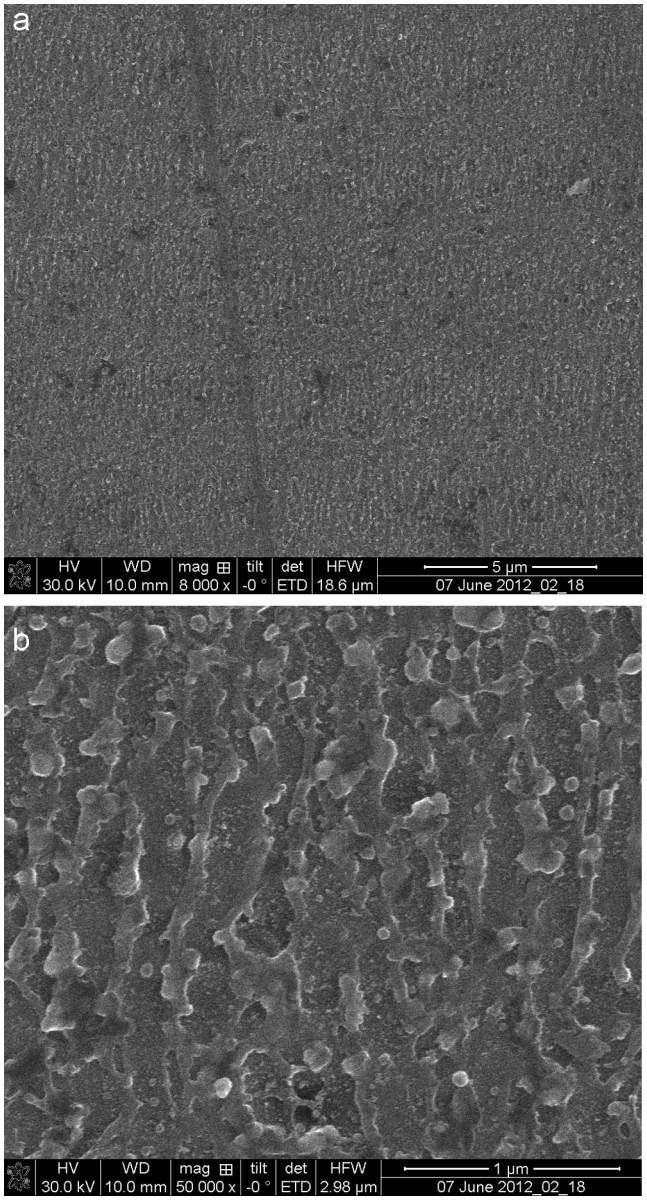

Fig. 8. Low number of pulses (approximately 1.4) resulting in no observable nanoripples: (a) 8000× magnification in SEM and (b) zoomed to 50,000× magnification in the SEM where random surface roughness appears to resemble solidification of molten material

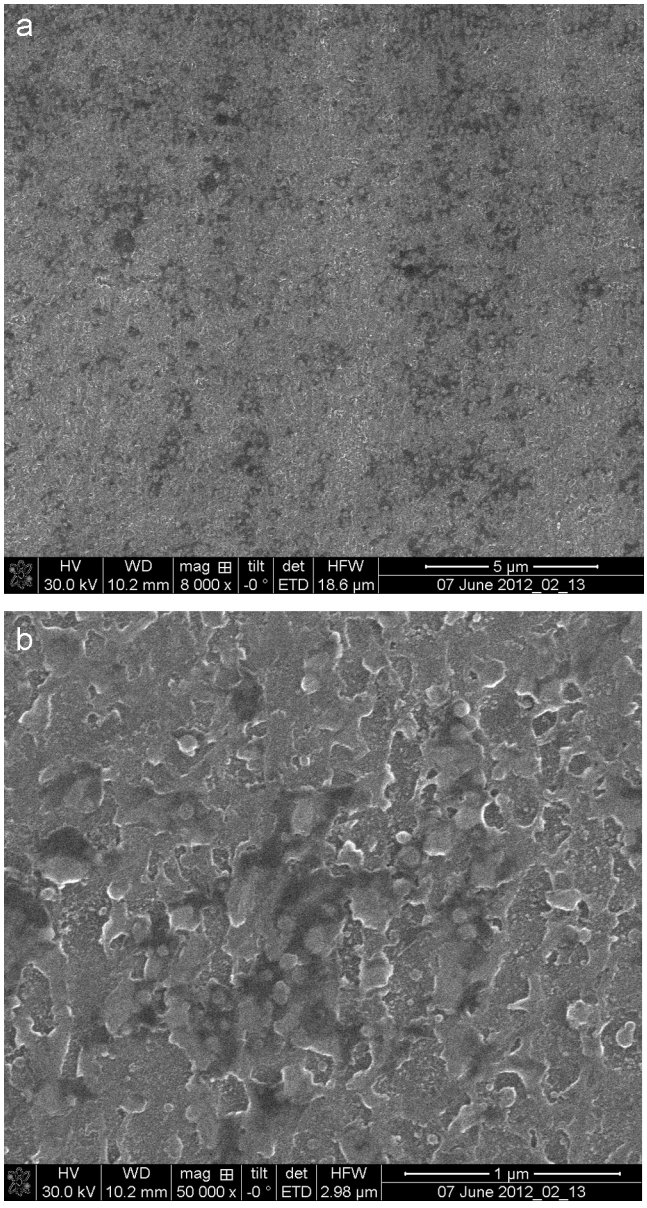

Fig. 9. Increased number of pulses (approximately 1.7) still presenting no periodic nanostructures (a) SEM at 8000× magnification and (b) SEM image at 50,000× magnification.

The sequence of images in Figs. 7–12 show the evolution of LIPSS from a polished surface, through random roughness and the emergence of LSFL. A globular roughness results from very few pulses and resembles solidified molten material. As LSFL emerge the surface roughness appears to alter with higher frequency roughness in the trenches between smoother ridges.

Using a line focus from a cylindrical lens can produce relatively wide regions in a single pass [30], as shown in Fig. 13. In this figure white light was incident at an angle of inclination large enough to allow one of the first diffraction orders to propagate from the surface, which is captured by a colour camera where a spectrum was recorded; the background is dark as the zeroth order does not enter the camera aperture. The horizontal variations in this picture result from the Gaussian profile of the laser beam. The vertical variations, meanwhile, are due to non-uniform illumination and large scale surface undulations. A top-hat corrector may improve feature consistency across the width.

SEM micrographs in Fig. 14 show LIPSS features on Sankvik Chromflex 7C27Mo2 made by scanning the 2 mm × ~5 µm line focused beam at three speeds with pulse repetition rate of 5 kHz. A different laser was used but with nominally identical parameters to that used for earlier results, however the number of pulses required is somewhat different. In this case it is clear that about 10 pulses are required to create well-formed LIPSS with period ~650 nm; two longitudinal scratches are also visible with diagonal scratches faintly remaining. If the fluence is set below the ablation threshold then LIPSS can be achieved but many more pulses are required.

Below the micrographs in Fig. 14 are Fourier transforms to highlight periodicity and its direction. For reference there is a circle

Please cite this article in press as: M. Ardron, et al., A practical technique for the generation of highly uniform LIPSS, Appl. Surf. Sci. (2014), http://dx.doi.org/10.1016/j.apsusc.2014.05.154

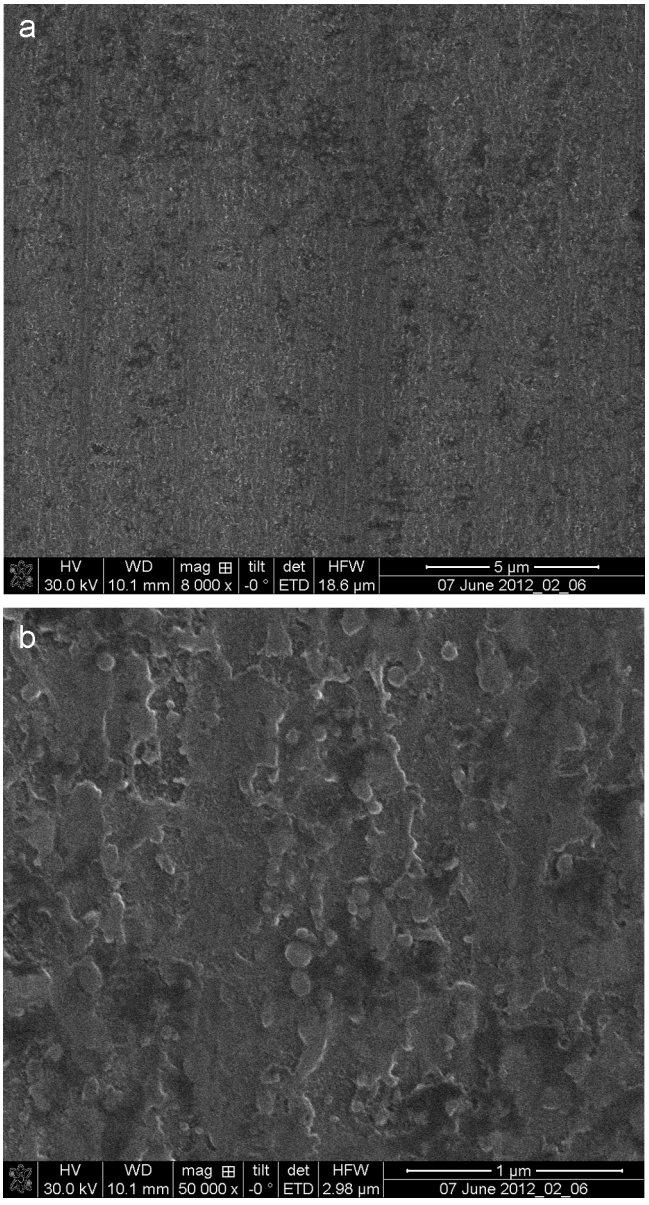

Fig. 10. Approximately 2.3 pulses, still no nanostructures (a) SEM 8000× magnification and (b) SEM 50,000× magnification.

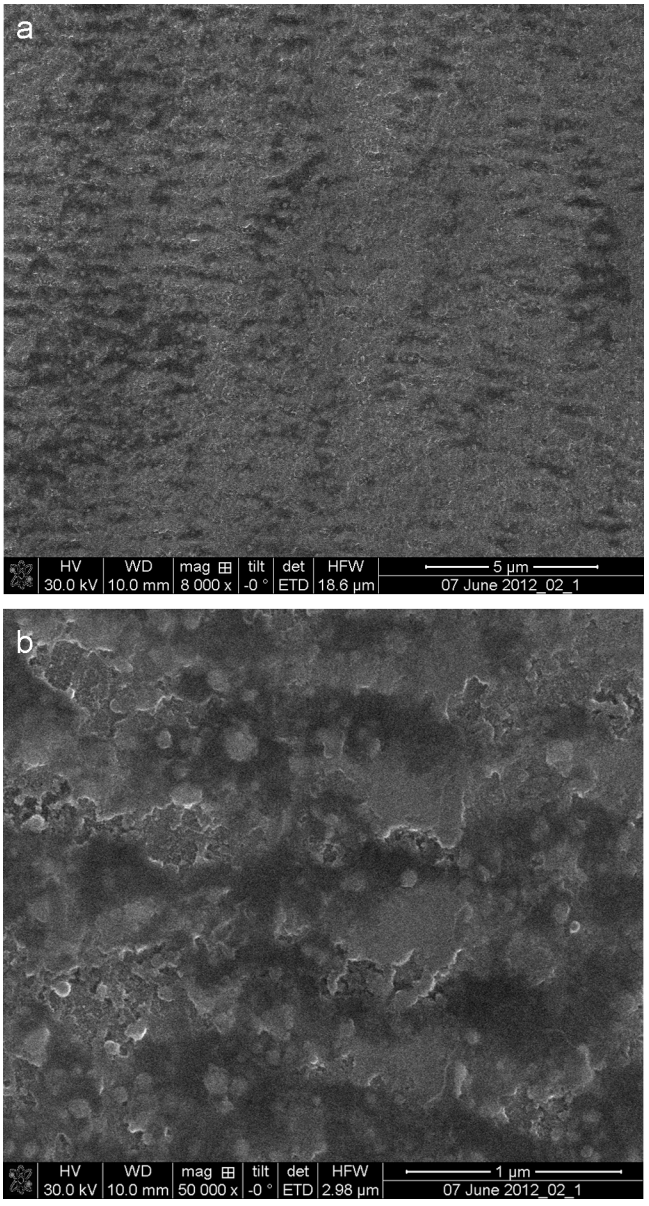

Fig. 11. Approximately 3.8 pulses and ripples are starting to emerge (a) nanoripples visible at 8000× magnification and (b) rough surface remains with nanoripple formation seen at 50,000×.

representing the incident laser wavenumber. Low pulse numbers gave emerging LSFL near to the incident frequency and aligned over a broad range centred roughly on the direction of the incident E-field; the orthogonal bright cloud within the laser frequency shows the polishing marks and breaks along the length of the ripple features. More pulses, shown in the middle image, give more distinct LSFL at slightly higher frequency and more consistently aligned with the E-field. In the right image are well defined periodic features with considerably higher spatial frequency than the incident light; the small bright spots showing well defined periodicity and direction aligned with the incident E-field. Polishing marks reduced as the pulse number increased as seen by the orthogonal scatter in the left FT image condensing to a central DC spot in the right FT image.

5. Discussion

Using the large pulse energy of about 0.1 mJ to visibly damage an area of 5 µm × 2 mm, well defined LSFL emerged after about 10 pulses although only random roughness appeared on an initially smooth surface after the first pulse or two. Even though EFT predicts peaks in the efficacy factor over crescent shaped regions with approximate radius corresponding to the laser frequency, the smooth surface was predicted to have no preferrential absorption in the absence of overlapping roughness components. Our experimental results agree with this prediction.

LIPSS start to appear with spatial period of the free space wavelength of the incident light and get progressively finer over the next few pulses; over this range of length-scale the initial surfaces were remarkably smooth in one direction using this crude preparation process. The EFT indicates that the formation mechanism

Please cite this article in press as: M. Ardron, et al., A practical technique for the generation of highly uniform LIPSS, Appl. Surf. Sci. (2014), http://dx.doi.org/10.1016/j.apsusc.2014.05.154

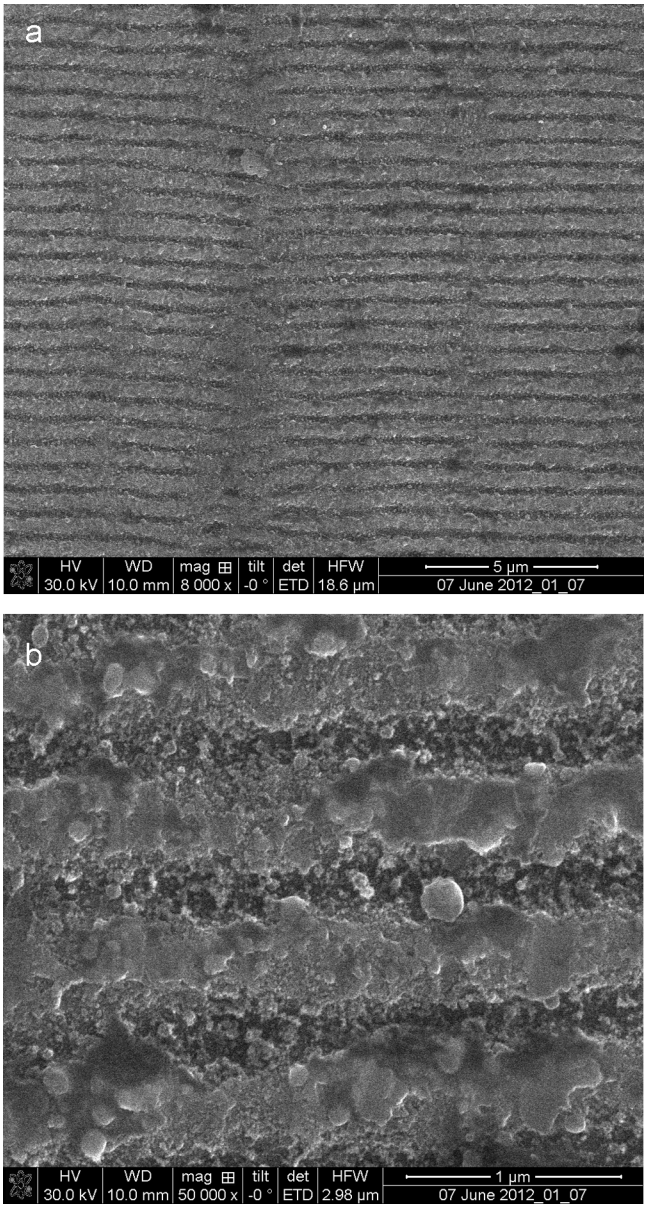

Fig. 12. Approximately 4.6 pulses and ripples are well established (a) at 8000× magnification ripples show a horizontal line of discontinuity probably scratch on substrate and (b) troughs show finer roughness than peaks at 50,000× magnification.

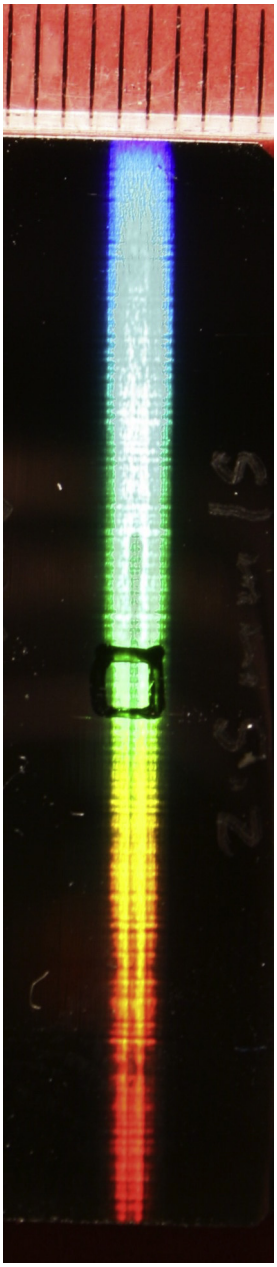

Fig. 13. Diffraction pattern from periodic structures on stainless steel made by line focus of ~740 mW beam with 5 kHz repetition rate travelling at 2.5 mm/s. Image illumination by tungsten filament bulb and image taken with large depth of field & slow shutter on a DSLR camera. The square in the centre is the region containing the SEM imaged region. The top shows 1 mm spaced lines for scaling. At focus the line was in the *x*-direction and scanned in the *y*-direction; polishing was performed along the *y*-direction.

behind LIPSS is the result of the electromagnetic field structure due to the incident pulse on the solid material interacting with the surface roughness [24] (EFT is time independent so it is not intended to be a comprehensive model.) This being the case, highly periodic features only require that the initial surface is devoid of topographical spatial frequencies in the region of spatial frequency peaks in the efficacy factor. This means that the initial surface preparation procedure needs to only achieve this goal, which can be provided by a simple linear (rather than circular) polishing process.

We have demonstrated a reliable method of producing relatively large areas of periodic nanostructures at 5 $mm^2\ s^{-1}$ for the laser processing part. In practice linear polishing with a spinning cloth wheel is a simple and versatile method of finishing a solid surface and adaptable to non-planar objects. When nano-texturing moulding or replication tools the surface can be appropriately prepared by polishing in the direction orthogonal to the direction of intended periodic features; that is polishing along the axis to which the E-field will be aligned during processing.

By rotating the polarisation through 90° we formed LIPSS aligned with the polishing direction and these can be seen in Fig. 1 where features show poor uniformity as polishing marks appear to disrupt the structured ablation field. The apparent doubling of the spatial frequency seen here was explained by field migration of half a feature period (quarter of the amplitude periodic structure) occurring after ablation of the initial LIPSS to a characteristic depth [31].

Please cite this article in press as: M. Ardron, et al., A practical technique for the generation of highly uniform LIPSS, Appl. Surf. Sci. (2014), http://dx.doi.org/10.1016/j.apsusc.2014.05.154

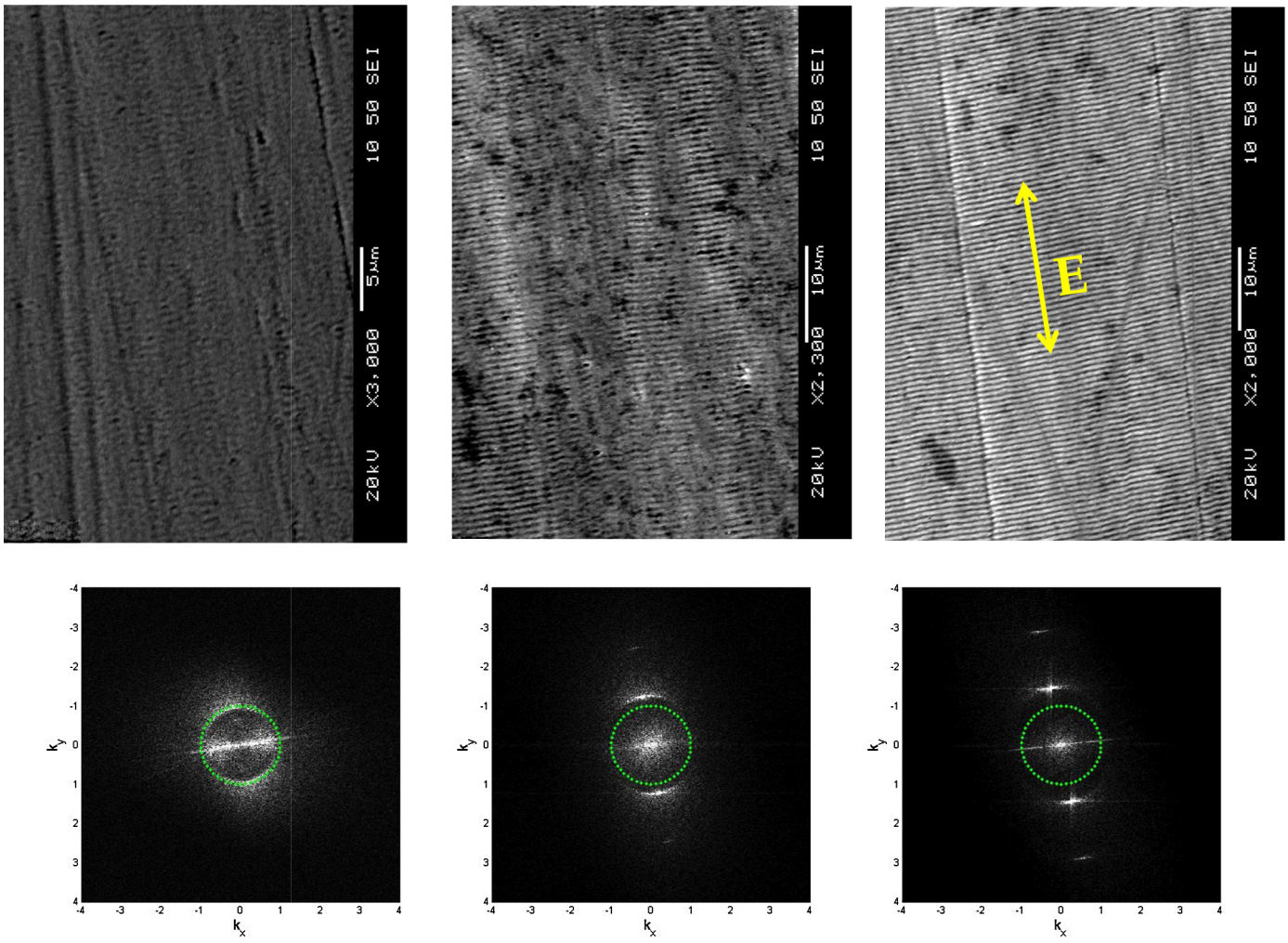

Fig. 14. SEM images showing the development of LIPSS features on Sankvik Chromflex 7C27Mo2. (a) Top left, scan speed of 4.5 mm/s ($N \approx 5.6$ pulses); (b) top middle, 3.5 mm/s ($N \approx 7$ pulses); and (c) top right, 2.5 mm/s ($N \approx 10$ pulses). Arrow shows alignment of the incident E-field. Lower three images are the corresponding Fourier transforms with dotted circles at $|k| = 1$.

6. Conclusions

We have demonstrated experimentally, and with reference to theory, that it is not necessary to start with a perfectly polished surface to generate highly uniform LIPSS. Instead, the substrate surface finish needs to only avoid features with vector spatial frequencies close to those of the intended LIPSS. An appropriate finish was provided by a high speed and low cost process: linear polishing with a spinning cloth wheel. This provides good surface finish on the length scale of the period of typical LIPSS. Setting the fluence to just above the single pulse ablation threshold allowed rapid formation of these features and use of line focused light successfully generated a comparatively large area with a single pass at a rate of 5 $mm^2\ s^{-1}$, with a laser repetition rate of only 5 kHz; a process found to be highly repeatable.

References

[1] J. Bonse, J. Krüger, Pulse number dependence of laser-induced periodic surface structures for femtosecond laser irradiation of silicon, J. Appl. Phys. 108 (2010) 034903, http://dx.doi.org/10.1063/1.3456501.
[2] P. Mannion, J. Magee, E. Coyne, G. O'Connor, T. Glynn, The effect of damage accumulation behaviour on ablation thresholds and damage morphology in ultrafast laser micro-machining of common metals in air, Appl. Surf. Sci. 233 (2004) 275–287, http://dx.doi.org/10.1016/j.apsusc.2004.03.229.
[3] P. Bizi-bandoki, S. Benayoun, S. Valette, B. Beaugiraud, E. Audouard, Applied surface science modifications of roughness and wettability properties of metals induced by femtosecond laser treatment, Appl. Surf. Sci. 257 (2011) 5213–5218, http://dx.doi.org/10.1016/j.apsusc.2010.12.089.
[4] W.L. Barnes, A. Dereux, T.W. Ebbesen, Surface plasmon subwavelength optics, Nature 424 (2003) 824–830.
[5] J. Eichstädt, G.R.B.E. Römer, a.J.H. in't Veld, Towards friction control using laser-induced periodic surface structures, Phys. Procedia 12 (2011) 7–15, http://dx.doi.org/10.1016/j.phpro.2011.03.099.
[6] D.C. Emmony, R.P. Howson, L.J. Willis, Laser mirror damage in germanium at 10.6 μm, Physics (College Park, MD) 598 (1973) 11–14, http://dx.doi.org/10.1063/1.1654761.
[7] A.-M. Kietzig, S.G. Hatzikiriakos, P. Englezos, Ice friction: the effects of surface roughness, structure, and hydrophobicity, J. Appl. Phys. 106 (2009) 024303, http://dx.doi.org/10.1063/1.3173346.
[8] B. Wu, M. Zhou, J. Li, X. Ye, G. Li, L. Cai, Superhydrophobic surfaces fabricated by microstructuring of stainless steel using a femtosecond laser, Appl. Surf. Sci. 256 (2009) 61–66, http://dx.doi.org/10.1016/j.apsusc.2009.07.061.
[9] R. Le Harzic, D. Dörr, D. Sauer, F. Stracke, H. Zimmermann, Generation of high spatial frequency ripples on silicon under ultrashort laser pulses irradiation, Appl. Phys. Lett. 98 (2011) 211905, http://dx.doi.org/10.1063/1.3593493.
[10] A. Borowiec, H.K. Haugen, Subwavelength ripple formation on the surfaces of compound semiconductors irradiated with femtosecond laser pulses, Appl. Phys. Lett. 82 (2003) 4462, http://dx.doi.org/10.1063/1.1586457.
[11] D. Du, X. Liu, G. Korn, J. Squier, G. Mourou, Laser-induced breakdown from 7 ns to 150 fs by impact ionization in SiO_2 with pulse widths, Appl. Phys. Lett. 64 (1994) 3071–3073.
[12] M. Birnbaum, Semiconductor surface damage produced by ruby lasers, J. Appl. Phys. 36 (1965) 3688.
[13] J. Bonse, A. Rosenfeld, J. Krüger, On the role of surface plasmon polaritons in the formation of laser-induced periodic surface structures upon

Please cite this article in press as: M. Ardron, et al., A practical technique for the generation of highly uniform LIPSS, Appl. Surf. Sci. (2014), http://dx.doi.org/10.1016/j.apsusc.2014.05.154

irradiation of silicon by femtosecond-laser pulses, J. Appl. Phys. 106 (2009) 104910, http://dx.doi.org/10.1063/1.3261734.
[14] G.N. Maracas, G.L. Harris, C.a. Lee, R.a. McFarlane, On the origin of periodic surface structure of laser-annealed semiconductors, Appl. Phys. Lett. 33 (1978) 453, http://dx.doi.org/10.1063/1.90376.
[15] J.E. Sipe, J.F. Young, J.S. Preston, Laser-induced periodic surface structure. I. Theory, Phys. Rev. 27 (1983) 1141–1154.
[16] J.Z.P. Skolski, G.R.B.E. Römer, J.V. Obona, V. Ocelik, a.J.H. in't Veld, J.T.M. De Hosson, Laser-induced periodic surface structures: fingerprints of light localization, Phys. Rev. B 85 (2012) 075320, http://dx.doi.org/10.1103/PhysRevB.85.075320.
[17] J. Young, J. Preston, H. van Driel, J. Sipe, Laser-induced periodic surface structure. II. Experiments on Ge, Si, Al, and brass, Phys. Rev. B 27 (1983) 1155–1172, http://dx.doi.org/10.1103/PhysRevB.27.1155.
[18] M. Csete, S. Hild, A. Plettl, P. Ziemann, Z. Bor, O. Marti, The role of original surface roughness in laser-induced periodic surface structure formation process on poly-carbonate films, Thin Solid Films 454 (2004) 114–120, http://dx.doi.org/10.1016/j.tsf.2003.11.086.
[19] J. Vincenc Obona, V. Ocelík, J.Z.P. Skolski, V.S. Mitko, G.R.B.E. Römer, a.J.H. in't Veld, et al., On the surface topography of ultrashort laser pulse treated steel surfaces, Appl. Surf. Sci. 258 (2011) 1555–1560, http://dx.doi.org/10.1016/j.apsusc.2011.09.130.
[20] J.M. Elson, R.H. Ritchie, Photon, interactions at a rough metal surface, Phys. Rev. B 4 (1971) 4129–4138.
[21] H. Raether, Surface Plasmons on Smooth and Rough Surfaces and on Gratings, Springer-Verlag, Berlin Heidelberg, 1988.
[22] A. Iron, T I.'C, Distribution (1977).
[23] M. Fox, Optical Properties of Solids, second ed., Oxford University Press, Oxford, 2010.
[24] J.Z.P. Skolski, Modeling of laser induced periodic surface structures, Appl. Phys. 5 (2010) 1–6, http://dx.doi.org/10.2961/jlmn.2010.03.0015.
[25] J.F. Young, J.E. Sipe, H.M. van Driel, Laser-induced periodic surface structure. III. Fluence regimes, the role of feedback, and details of the induced topography in germanium, Phys. Rev. B 30 (1984) 2001–2015.
[26] Z. Guosheng, P.M. Fauchet, A.E. Siegman, Growth of spontaneous periodic surface structures on solids during laser illumination, Phys. Rev. B 26 (1982) 5366–5381.
[27] P.T. Mannion, J. Magee, E. Coyne, G.M.O. Connor, T.J. Glynn, The effect of damage accumulation behaviour on ablation thresholds and damage morphology in ultrafast laser micro-machining of common metals in air, Appl. Surf. Sci. 233 (2004) 275–287, http://dx.doi.org/10.1016/j.apsusc.2004.03.229.
[28] P. Mannion, J. Magee, E. Coyne, G. O'Connor, Ablation thresholds in ultrafast laser micromachining of common metals in air, in: SPIE 4876, Opto-Irel. 2002 Opt. Photonics Technol. Appl., SPIE, 2003.
[29] D.J.O. Orzi, F.C. Alvira, G.M. Bilmes, Determination of femtosecond ablation thresholds by using laser ablation induced photoacoustics (LAIP), Appl. Phys. A 110 (2012) 735–739, http://dx.doi.org/10.1007/s00339-012-7230-x.
[30] S.K. Das, K. Dasari, A. Rosenfeld, R. Grunwald, Extended-area nanostructuring of TiO_2 with femtosecond laser pulses at 400 nm using a line focus, Nanotechnology 21 (2010) 155302, http://dx.doi.org/10.1088/0957-4484/21/15/155302.
[31] J. Yao, C. Zhang, H. Liu, Q. Dai, L. Wu, S. Lan, et al., High spatial frequency periodic structures induced on metal surface by femtosecond laser pulses, Opt. Express 20 (2012) 6651–6656.

Please cite this article in press as: M. Ardron, et al., A practical technique for the generation of highly uniform LIPSS, Appl. Surf. Sci. (2014), http://dx.doi.org/10.1016/j.apsusc.2014.05.154